Redox Titration of All Electron Carriers of Cytochrome *c* Oxidase by Fourier Transform Infrared Spectroscopy†

Elena A. Gorbikova, Kai Vuorilehto, Mårten Wikström, and Michael I. Verkhovsky*

Program for Structural Biology and Biophysics, Institute of Biotechnology, University of Helsinki, PB 65 (Viikinkaari 1), FIN-00014 Helsinki, Finland

Received February 7, 2006; Revised Manuscript Received March 14, 2006

ABSTRACT: Electrochemical redox titrations of cytochrome *c* oxidase from *Paraccocus denitrificans* were performed by attenuated total reflectance Fourier transform infrared (ATR-FTIR) spectroscopy. The majority of the differential infrared absorption features may be divided into four groups, which correlate with the redox transitions of the four redox centers of the enzyme. Infrared spectroscopy has the advantage of allowing one to measure independent alterations in redox centers, which are not well separated, or even observed, by other spectroscopic techniques. We found 12 infrared bands that titrated with the highest observed midpoint redox potential (E_m = 412 mV at pH 6.5) and which had a pH dependence of 52 mV per pH unit in the alkaline region. These bands were assigned to be linked to the Cu_B center. We assigned bands to the Cu_A center that showed a pH-independent E_m of 250 mV. Two other groups of infrared differential bands reflected redox transitions of the two heme groups and showed a more complex behavior. Each of them included two parts, corresponding to high- and low-potential redox transitions. For the bands representing heme *a*, the ratio of high- to low-potential components was ca. 3:2; for heme a_3 this ratio was ca. 2:3. Taking into account the redox interactions between the hemes, these ratios yielded a difference in E_m of 9 mV between the hemes (359 mV for heme *a*; 350 mV for heme a_3 at pH 8.0). The extent of the redox interaction between the hemes (−115 mV at pH 8.0) was found to be pH-dependent. The pH dependence of the E_m values for the two hemes was the same and about two times smaller than the theoretical one, suggesting that an acid/base group binds a proton upon reduction of either heme. The applied approach allowed assignment of infrared bands in each of the four groups to vibrations of the hemes, ligands of the redox centers, amino acid residues, and/or protein backbone. For example, the well-known band shift at 1737/1746 cm^{-1} corresponding to the protonated glutamic acid E278 correlated with oxidoreduction of heme *a*.

Cytochrome *c* oxidase (C*c*O)[1] is a terminal transmembrane enzyme of the respiratory chain in mitochondria and aerobic bacteria. Its biological functions are to catalyze respiratory reduction of O_2 to water and to generate a transmembrane electrochemical potential, which is used for driving ATP synthesis. C*c*O includes four redox centers: Cu_A, heme *a*, heme a_3, and Cu_B. Cu_A is the primary electron acceptor from cytochrome *c*. Electrons are transferred from Cu_A through heme *a* to the binuclear reaction center, composed of heme a_3 and Cu_B, where the catalysis of O_2 reduction takes place. During the catalytic cycle the binuclear center passes through consecutive intermediate states, each stable intermediate state being generated after acceptance of one electron by the binuclear center. During one complete catalytic cycle, four electrons and four "chemical" protons are accepted by the binuclear center, with reduction of oxygen to two water molecules. Chemical protons are delivered from the matrix side in mitochondria or the cytosol in prokaryotic cells. At the same time, free energy from this reaction drives the pumping of another four protons across the membrane. These two mechanisms of electron and proton movements generate a transmembrane difference in electrochemical potential, which is necessary for the synthesis of ATP (for reviews see refs *1*−*4*).

The redox centers and their ligands undergo a series of structural alterations during electron and proton transfer. Some of these changes may take part in the mechanisms of the catalytic cycle and in transmembrane potential generation.

The structure of C*c*O was solved at a resolution of 2.7 Å for two subunits of the *Paracoccus denitrificans* enzyme and at 1.8−1.9 Å for the bovine heart enzyme (*5*, *6*), which is not enough to define the protonation status of redox centers and their ligands or the dipole orientation of water molecules. One of the most promising methods that allows more detailed information about structure, charge, and the environment of the redox centers is Fourier transform infrared (FTIR) spectroscopy (*7*). Attenuated total reflectance (ATR) FTIR spectroscopy has been used to measure changes in several

† This work was supported by the Academy of Finland (project numbers 200726 and 44895), Biocentrum Helsinki, and the Sigrid Jusélius Foundation. E.A.G. was supported by the Center of International Mobility (CIMO), Finland.

* To whom correspondence should be addressed. Phone: +358 9 191 58005. Fax: +358 9 191 59920. E-mail: michael.verkhovsky@helsinki.fi.

[1] Abbreviations: FTIR, Fourier transform infrared; ATR, attenuated total reflectance; C*c*O, cytochrome *c* oxidase; WE, working electrode; CE, counter electrode; RE, reference electrode; NHE, normal hydrogen electrode; E_m, midpoint redox potential (relative to NHE); ΔOD, difference in optical density; IR, infrared; red, reduced; ox, oxidized.

10.1021/bi060257v CCC: $33.50
Published on Web 04/08/2006

enzymes (*8*−*10*), including redox-induced changes (*8*, *11*, *12*). ATR-FTIR spectroscopy works on a protein film and allows for changing experimental parameters during the measurements (including redox potential and buffer) with the same sample film.

In the present study we report for the first time on full electrochemical redox titrations of *P. denitrificans* aa_3 oxidase monitored by ATR-FTIR spectroscopy. This allowed us to create a "Δ optical density−potential−wavenumber" surface, which was decomposed into separate titration curves at peaks and troughs of redox-induced difference FTIR spectra. All FTIR redox titration curves in the range of 4000−1000 cm^{-1} were sorted out into four groups and assigned to each of the four redox centers.

MATERIALS AND METHODS

Sample Preparation. Cytochrome *c* oxidase from *P. denitrificans* was extracted from culture as previously described (*13*) and dissolved in 20 mM Tris-HCl and 0.05% (w/v) β-dodecyl maltoside at pH 7.8. Oxidase was further purified by Source 15-Q ion-exchange chromatography to remove lipid contaminants. Production of a stable film for ATR-FTIR measurements required depletion of detergent content so that the sample became sufficiently hydrophobic (so-called "ATR-ready" sample) (*11*). The procedure of detergent depletion was essentially as described in ref *14*.

An ATR silicon microprism (Sens IR Technologies, three-bounce version, surface diameter 3 mm) was slightly polished with 0.05 μm aluminum powder to ensure appropriate sticking of the enzyme to the surface for the period of the experiment. The ATR-ready sample was thawed, and 10−20 μL was positioned on the prism surface and dried with a gentle flow of nitrogen gas until changes in FTIR spectra were no longer observed. The signal intensity of the amide I band of the semidried film was 0.9−1.2. Then the protein film was rewetted with titration buffer and covered with the chamber, which allowed continuous flow of buffer over the sample surface, driven by a peristaltic pump at a flow rate of 2 mL/min. In such conditions the protein film was stabilized for about 20 h.

Redox Titration and Electrochemistry. To control the redox potential, a homemade flow-by electrochemical cell (*15*) was used (Figure 1). Gold grains (diameter 0.3−0.5 mm) were used as the working electrode (WE), a platinum-plated titanium grid as the counter electrode (CE), and Ag/AgCl/saturated KCl as the reference electrode (RE). A titration buffer with mediators was continuously pumped through the working electrode to the ATR chamber. To restrict diffusion of oxygen from the counter electrode into the titration buffer, the CE was separated from the WE by two ion-exchange membranes and an additional 1 cm thick compartment, which was filled with 400 mM potassium phosphate buffer, pH 8.0, and continuously bubbled with nitrogen. The cell was connected to a Princeton Applied Research potentiostat, and the potential was set automatically by the software. To equilibrate the enzyme film with the potential of the working electrode, a set of three mediators was used: 1,2-diaminocyclohexane-*N*,*N*,*N*′,*N*′-tetraacetic acid + Fe, midpoint potential +95 mV; terpyridine$_2$ cobalt, +265 mV; ferrocene acetate, +370 mV. Each component was used at a concentration of 200 μM. Due to the large surface area of the working

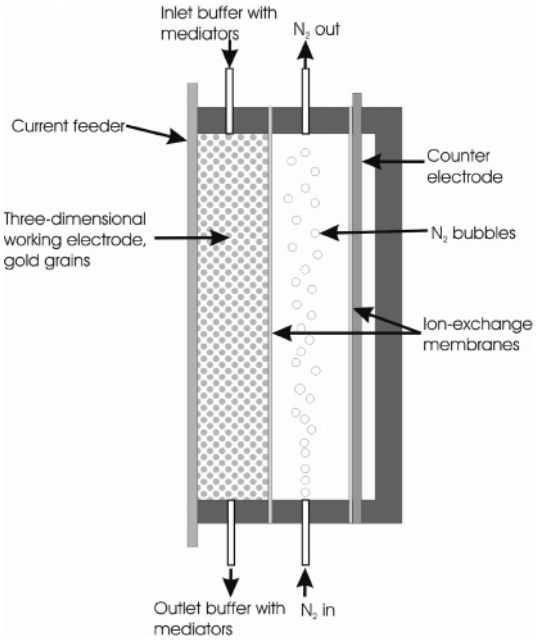

FIGURE 1: The flow-through electrochemical cell used to control the potential of C*c*O. The buffer with mediators was equilibrated with the working gold electrode when flowing through the cell.

electrode (about 300 cm^2) and continuous flow of mediator-containing buffer, the redox reactions of the enzyme proceeded very fast. The kinetics of the equilibration process was controlled spectrophotometrically in the visible range. In most cases no changes in optical density (OD) were observed after 10 min. The selected mediators were practically colorless and sufficiently stable in the pH and potential ranges used. Furthermore, they did not show any significant contribution to the FTIR or visible spectra.

The electrochemical cell was connected to the ATR cell by a 6 cm long Tygon tubing (extremely low oxygen permeability, 0.08 cm inner diameter). To be sure that the potentials in the ATR cell are the same as in the electrochemical cell, the redox potential of the liquid was controlled.

Redox titrations of cytochrome *c* oxidase were performed as follows. Initially, the enzyme was equilibrated at −300 mV (vs NHE). The titration was performed step by step, starting from +480 mV and going down to 0 mV in 40 mV steps. Each point was equilibrated for 15 min, after which visible and FTIR spectra were measured. After each high-potential point, the system was reequilibrated for 15 min at −300 mV in order to measure a new FTIR background and to reduce possible trace amounts of oxygen that could have leaked into the titration buffer.

To determine the pH dependence of the redox transitions of C*c*O, titrations were performed at three different pH values. Potassium phosphate buffer (200 mM) was used at pH 6.5 and 8.0 and 100 mM borate buffer at pH 9.0. K_2SO_4 (100 mM) was added to the borate buffer for better conductivity.

Spectroscopy. A Bruker IFS 66s FTIR spectrometer (equipped with an MCT detector) and a visible spectrophotometer USB2000 (Ocean Optics) were used. FTIR spectra were measured in the range 4000−1000 cm^{-1} with 4 cm^{-1} spectral resolution and scanner frequency 40 kHz; the number of scans in background and sample spectra was 512; apodization function, Blackman-Harris 3-Term. Visible

spectra were measured in the range 400−650 nm. The light guide of the spectrophotometer was connected to the ATR cell, which allowed simultaneous collection of FTIR and visible spectra.

Before the titration started, the backgrounds in the visible and infrared (IR) regions were measured at the initial potential (−300 mV). Every potential step with equilibration was followed by collecting sample spectra in the visible and sample and new background spectra in the IR region. This data acquisition system produced one oxidized-minus-reduced (ox-red) and one reduced-minus-oxidized (red-ox) FTIR difference spectrum and one ox-red visible spectrum per applied potential step. All measurements were performed at room temperature.

The whole titration process (initializing, sending commands to/from Ocean Optics and FTIR Opus software, and collecting data) was controlled by Titrator software designed in our laboratory by Nikolay Belevich.

Data Analysis. Every ox-red FTIR difference spectrum was averaged with the corresponding red-ox spectrum. FTIR Δ optical density−potential−wavenumber surfaces for three pH values were generated. Redox titration curves (dependence of ΔOD on applied potential at peaks and troughs) were extracted from the surfaces in the region 4000−1000 cm^{-1}. The FTIR titration curve extraction was carried out in two steps. In the first step, determination of intensity of every peak (and trough) was defined as the difference between the intensity at the peak (trough) and half the sum of the intensities of the adjacent troughs (peaks). After this procedure, the sum of the extracted titration curves was divided into groups. In the second step, the assignment of each peak and trough to each group was verified. This time the intensity of a peak (trough) was calculated as the difference between the intensity at the peak (trough) and half the sum of the intensities at ±3 cm^{-1} distance from the peak (trough). This approach helps to avoid ambiguity in the assignment of peaks and adjacent troughs. All further calculation and fitting procedures were performed in Matlab software.

RESULTS

Spectroelectrochemical FTIR Titrations of CcO. The redox titrations were performed by a combination of an electrochemical and a spectroscopic approach in the potential range 0:+480 mV vs NHE, with a step of 40 mV, as described in Materials and Methods. After each measurement point, the system was reequilibrated at −300 mV and then poised at the next measuring point shifted by 40 mV from the previous one. At each step, visible and infrared spectra were collected. Almost no changes in the FTIR or visible region were observed between −300 and 0 mV. Two sets of titration data at each pH value were averaged to obtain the final data for further analysis.

Figure 2 shows a typical Δ optical density−potential−wavenumber surface in the 1800−1000 cm^{-1} region; the surface was generated by collecting the electrochemically induced difference FTIR spectra as a function of the applied redox potential. The electrochemically induced fully reduced minus fully oxidized difference FTIR spectra of C*c*O had the same features as those published earlier (*14*, *16*−*18*). Titration curves were extracted at every maximum and minimum of the FTIR surface. The same FTIR surface for the infrared region 4000−2500 cm^{-1} is presented in Figure 3.

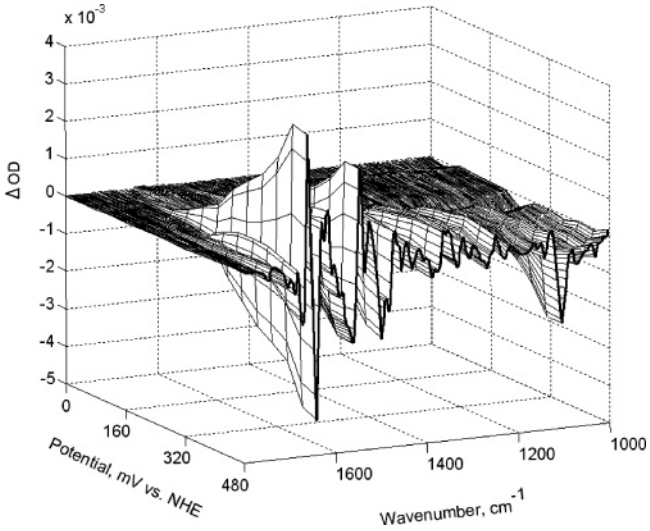

FIGURE 2: Typical surface Δ optical density−potential−wavenumber in the infrared region 1800−1000 cm^{-1}. The surface is a development of reduced-minus-oxidized difference FTIR spectra depending on potential. Applied potentials are in the range of +480:0 mV vs NHE with a step of 40 mV. For other conditions see Results.

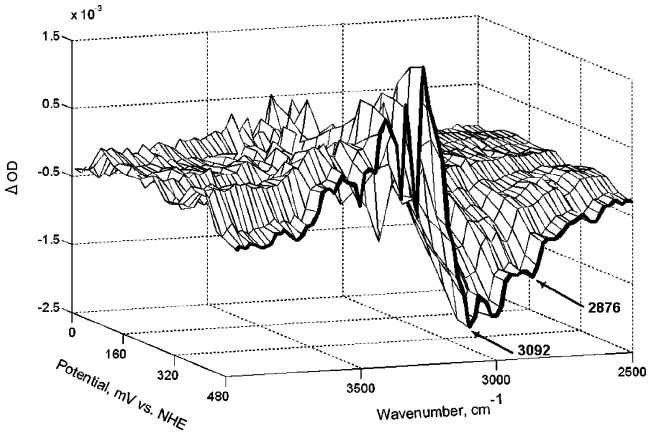

FIGURE 3: The Δ optical density−potential−wavenumber surface in the 4000−2500 cm^{-1} infrared region. The surface is a development of reduced-minus-oxidized FTIR spectra depending on potential. Applied potentials are in the range of +480:0 mV vs NHE with a step of 40 mV.

The development of the typical visible red-ox difference spectra (recorded simultaneously with FTIR spectra) is shown at Figure 4. The main contributors in the spectral range 400−650 nm are hemes *a* and a_3. To define the number of redox-active components, analysis of the first derivative of the Δ optical density measured at different wavelengths along the redox potential axis brought out three maxima, corresponding to three redox components in the data set at each pH. These data show two major components (cf. ref *26*) with apparent E_m values of ca. 400, 360, 280 mV and 240, 200, 200 mV for pHs 6.5, 8.0, 9.0 and a minor one (~5%) with an E_m of ca. 120 mV at all three pH values. The minor component has a peak at 590 nm and most likely reflects a small fraction of low-spin heme a_3 produced during protein film preparation and/or its interaction with products of the decay of redox mediators.

Assignment of FTIR Redox Titration Curves in the 1800−1000 cm^{-1} Region. Practically all infrared bands were complex, but with one major component in each. The interpretation of the FTIR titration curves is based on the

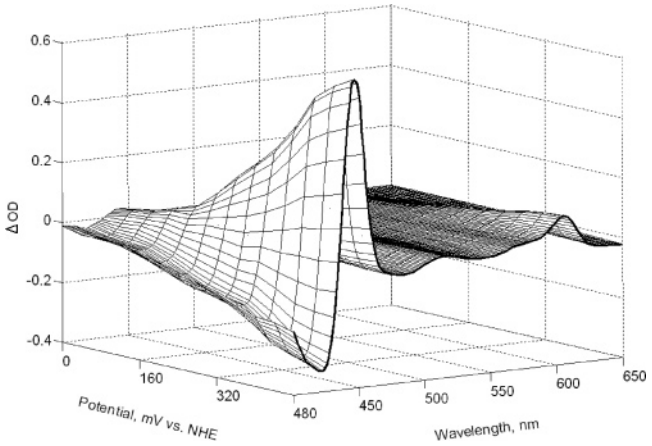

FIGURE 4: Development of the visible difference (reduced-minus-oxidized) spectra (400−650 nm) of cytochrome *c* oxidase during redox titration from +480 to 0 mV vs NHE with a step of 40 mV.

fact that the 1800−1000 cm^{-1} infrared region consists of vibrational modes of the heme groups and the ligands directly bound to the four redox centers and to other groups reflecting the redox changes indirectly.

The whole population of redox titration curves fell into four groups according to their behavior. During the analysis, all data from the same group were normalized to the maximum amplitude and averaged, and the averaged points were fitted. In one of the four groups, the experimental points could be well fitted with a simple Nernstian curve for a one-electron transition (Figure 5D). In the other three groups the experimental points exhibited more complicated behavior with two apparent redox transitions (Figure 5A−C).

For bovine C*c*O an anticooperative effect in the reduction of the hemes is known (*19*, *20*). As a result, the redox titration curve of each heme is split into two components: a high- and a low-potential transition (*19*, *20*). Panels A and B of Figure 5 show two populations of titration curves of FTIR features with such a splitting into high- and low-potential parts. The ratio of amplitudes (high potential/low potential) of those components was ca. 3:2 for the first group of curves (Figure 5A) and 2:3 for the second one (Figure 5B). On the basis of optical spectroscopy (see also Bloch et al., to be submitted for publication), we have found that the high-potential part contains a slightly larger contribution of heme *a* vs heme a_3 and vice versa for the low-potential part. Hence, we assigned the curves presented in Figure 5A to infrared features coupled to oxidoreduction of heme *a* and the curves presented in Figure 5B to heme a_3 (see also Bloch et al., to be submitted for publication).

We applied the "neoclassical model" (*19*) to fit data points of these first two groups. This model describes titration of a system of two redox centers with a redox interaction between them. The high-asymptotic potentials (reflecting the midpoint potentials of the hemes without interaction), the extent of anticooperativity, and the apparent midpoint potentials for the high- and low-potential transitions were found from the fit for both hemes. As follows from the model, these apparent E_m values for high- and low-potential transitions were the same for hemes *a* and a_3. The high-potential transition had E_m values of 405, 372, and 342 mV at pH 6.5, 8.0, and 9.0; the low-potential values were correspondingly 238, 222, and 221 mV. The fit of these data resulted in high-asymptotic potentials of 391, 359, and 330 mV for heme *a*, and 383, 350, and 320 mV for heme a_3 at the investigated pH values. The fit also showed that the equilibrium constant of electron transfer between the two hemes is pH-independent in the investigated pH range but that the anticooperative redox interaction between them depends significantly on pH. The extent of this interaction was found to be −132, −115, and −86 mV at the measured pH values.

The pH dependence of the high-potential E_m values for the two hemes was the same, viz., ∼30 mV/pH unit, which is one-half of the theoretical value for uptake of one proton on reduction. Such a dependence is expected if the two hemes share a group that binds a proton upon reduction of either heme (cf. ref *20*).

We assigned the third group of curves to the reduction of Cu_B (Figure 5C), with E_m values of the high-potential transition of 412, 366, and 314 mV at pH 6.5, 8.0, and 9.0. The pH dependence of these curves was 52 mV/pH at alkaline conditions, which is close to the theoretical one. However, there is also a low-potential wave contributing by 20−33% and with a pH-independent E_m of ca. 220 mV (Figure 5C). It is possible that this reflects a redox interaction between Cu_B and either or both of the heme groups. More data are required to test this possibility, but in this work we have chosen to initially apply the simplest model where only the heme−heme interaction is considered. Another possible explanation for the low-potential wave in Figure 5C is that vibrational modes reflecting reduction of centers with a pH-independent midpoint potential in this region (low-potential heme or Cu_A) are in the same wavenumber region as those sensing the Cu_B redox changes.

The fourth population of the FTIR titration curves (Figure 5D) was pH-independent with an E_m of 250 mV. We assigned these transitions to Cu_A because the E_m value is close to that found for this center in *P. denitrificans* (*21*) and bovine C*c*O (*22*). For the bovine enzyme it was also found to be largely pH-independent (*22*).

Furthermore, there was a population of titration curves that had no systematic redox/pH behavior. The first reason for this is a low signal-to-noise ratio. The second is that these bands are the result of overlapping bands originating from different redox centers. Because of obscurity of their origin these bands were not analyzed or assigned.

Midpoint potentials of Cu_B and of the high-potential components of heme *a* and a_3 are located in a potential range higher than 400 mV at pH 6.5. Normalization of data points at maximal amplitude, together with the fact that the titration was performed with the high-potential limit of only 480 mV, could cause an erroneous shift of these E_m values (at pH 6.5) in the direction of lower potentials.

The values of midpoint redox potentials and anticooperative interaction of redox centers are listed in Table 1, and assignments of the resolved peaks to direct and indirect ligands of the redox centers and to heme vibrations in the region 1800−1000 cm^{-1} are systematized in Table 2a.

Figure 6 represents different contributions of bands, assigned to all four redox centers, into difference FTIR spectra. The complete red-ox spectrum in Figure 6A, obtained as a difference between −300 and +480 mV, contains the redox transitions of all four redox centers. However, at different potential levels the contribution of each redox center varies. The biggest diversities are seen at pH

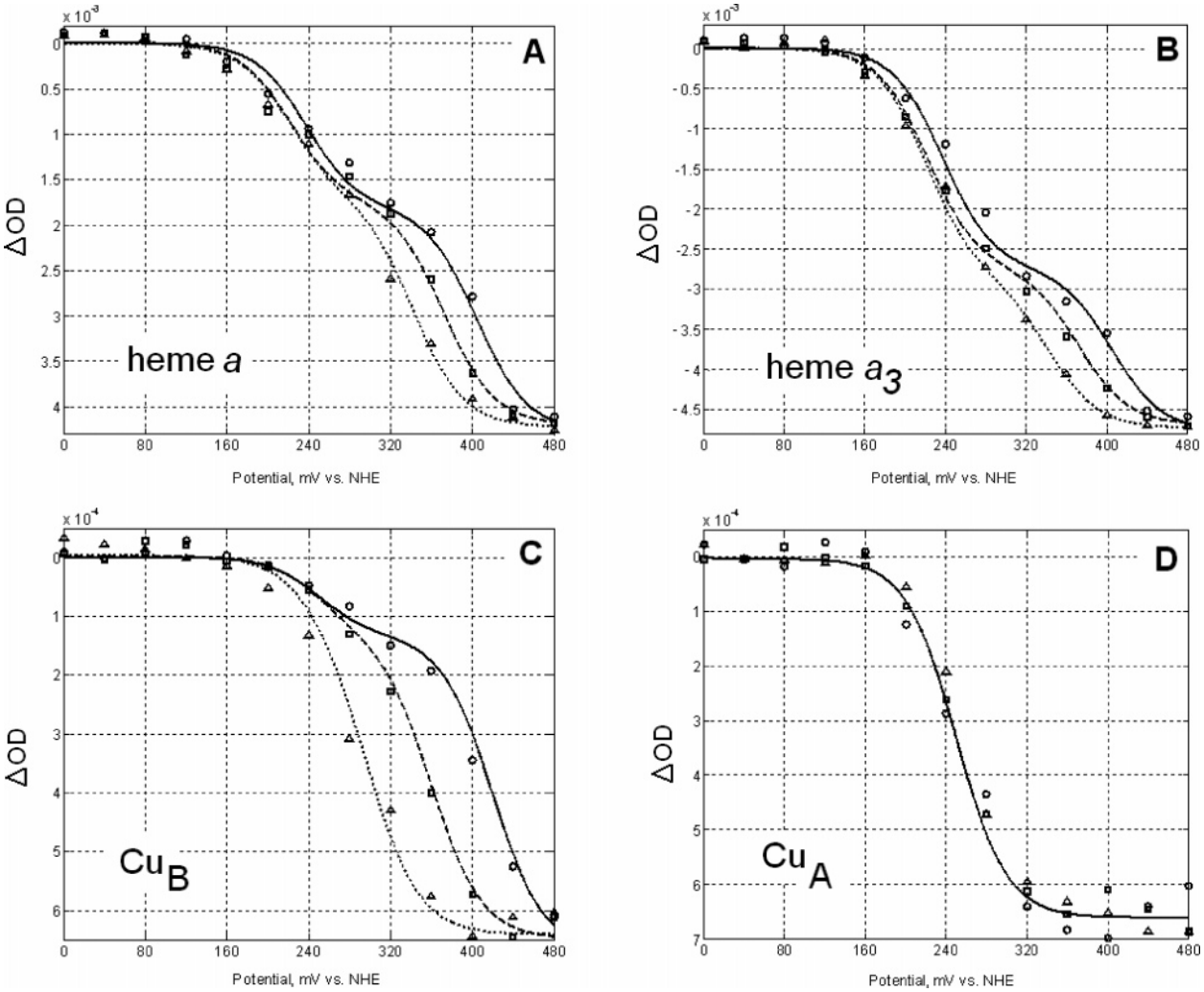

FIGURE 5: Four patterns of redox titration curves extracted from FTIR surfaces. Redox titration curves at three pH values are presented: circles and solid line, pH 6.5; squares and dashed line, pH 8.0; triangles and dotted line, pH 9.0. Pattern assigned to the redox transitions of (A) heme *a*, (B) heme a_3, (C) Cu_B, and (D) Cu_A. Extracted titration curves with the same behavior were averaged and fitted (for details see text). Resulting theoretical curves were plotted together with experimental points of one characteristic curve in each pattern [band at 1661 cm^{-1} for (A), 1641 cm^{-1} for (B), 1489 cm^{-1} for (C), and 1603 cm^{-1} for (D)].

Table 1: Estimated Values of Midpoint Redox Potentials of Electron Transfer Cofactors of C*c*O from *P. denitrificans* and Anticooperative Interaction between Them Based on Electrochemical Titration by FTIR Spectroscopy

	pH		
redox component, mV	6.5	8.0	9.0
high-potential heme transition	405	372	342
low-potential heme transition	238	222	221
heme *a*, high-asymptote redox potential	391	359	330
heme a_3, high-asymptote redox potential	383	350	320
heme a/a_3 anticooperative interaction	−132	−115	−86
Cu_B	412	366	314
Cu_A	250	250	250

6.5. The spectra at the potential step from +360 to +400 mV (Figure 6B) are dominated by Cu_B and main changes linked to heme *a*; Cu_A and heme a_3 transitions are poorly presented. At the same time, the potential step from +280 to +320 mV (Figure 6C) mainly includes transitions linked to heme a_3 and Cu_A and a smaller portion of transitions linked to heme *a* and Cu_B.

Assignment of FTIR Titration Curves in the 4000−2500 cm^{-1} Region. The development of a typical FTIR ox-red spectrum in the 4000−2500 cm^{-1} region is shown in Figure 3. This so-called "water region" is noisy because of very strong absorption from water O−H vibrations in liquid and semiliquid samples. To be able to analyze this region, spectra were smoothed and redox titration curves extracted. The redox titration curves at two peaks were sufficiently resolved to assign them to the patterns mentioned above. These curves, with minima at 3092 and 2876 cm^{-1} (Figure 3), showed the behavior of Cu_B oxidoreduction. Hence, these vibrational modes may, for example, be due to NH modes of the histidine or OH^- ligands of Cu_B (see Table 2b) but could also be due to reorientation of the dipole moments of water molecules. A tentative assignment of the peaks in the 4000−2500 cm^{-1} region is shown in Table 2b.

In addition to differential bands due to single diatomic groups, the water region includes a redox-dependent shift of a wide continuum (Figure 3). To be able to extract titration curves of the continuum shift, the spectra were highly smoothed. Redox titration curves of this shift were calculated as the difference between the minimum at ca. 3040 cm^{-1} and the maximum at ca. 3280 cm^{-1}. Figure 7 shows this redox titration curve at pH 8.0. The E_m of this curve was 335 mV and showed no significant pH dependence. The shift of the continuum band might be speculatively assigned to

Table 2: Linkage of FTIR Bands to Oxidoreduction of Individual Redox Centers and Tentative Assignment of the Infrared Vibrations[a]

band position, cm^{-1}	redox center	redox state	band assignment (absorber; vibration type; tentative residue)[b]
		(a) 1800−1000 cm^{-1} Region	
1746/1737	heme *a*	ox/red	E, Glu-COOH; ν(C═O); E278 (*28*)
1689	Cu_A	ox	amide I, β-sheet; ν(C═O)
1684	Cu_A	red	amide I, β-sheet; ν(C═O)
1674	heme a_3, complex band	ox	R, Arg-H_5^+; $\nu_{as}(CN_3H_5^+)$; R473 (*28*)/propionate; ν(C═O) (*18*)/formyl (*29*)/amide I, turns; ν(C═O)
1661	heme *a*	red	amide I, α-helix; ν(C═O)/amide I, turns; ν(C═O)
1655	heme a_3	ox	amide I, α-helix; ν(C═O)
1651	Cu_A	red	amide I, α-helix; ν(C═O)
1641	heme a_3	ox	formyl; ν(C═O) (*11*)/amide I, β-sheet; ν(C═O)
1630	heme a_3	red	R, Arg-H_5^+; $\nu_s(CN_3H_5^+)$; R473/H, $HisH_2^+$; ν(C═C); H403 (*28*)/formyl (*29*)/amide I, β-sheet; ν(C═O)
1618	heme a_3	red	Y, Tyr-OH; ν(CC) ring, δ(CH); Y280/W; ν(CC), ν(C═C); W272, W164 (*28*)/vinyl; ν(C−C) (*26*)/amide I, β-sheet, ν(C═O)
1603	Cu_A	red	amide I, β-sheet; ν(C═O)
1592	Cu_A	ox	H, HisH; ν(C═C); H224, H181/R, Arg-H_5^+; $\nu_{as}(CN_3H_5^+)$; R473/D, Asp-COO^-; $\nu_{as}(COO^-)$; D178 (*28*)
1561	heme a_3	ox	W, Trp-NH; ν(CC), δ(CH); W164 (*28*)/propionate (*18*)
1546	heme *a*	red	heme; ν_{38y} (*26*)
1537	heme *a*	ox	propionate (*18*)
1526	heme a_3	red	propionate/heme; ν_{38s}/heme; ν_{38y} (*26*)
1510	Cu_A	red	W, Trp-NH; ν(CN), δ(CH), δ(NH); W121 (*28*)
1489	Cu_B	red	W; ν(CC), δ(CH); W272/H, HisH; ν(C═N), δ(CH); H325, H326 (*28*)
1483	Cu_B	ox	W, Trp-NH; ν(CC), δ(CH); W272 (*28*)
1473	heme a_3	red	F; $\delta_{as}(CH_3)$; F412 (*28*)/heme; A_{1g},ν_3 (*29*)
1468	Cu_A	ox	W, Trp-NH; δ(CH), ν(CC), ν(CN); W121 (*28*)
1455	Cu_B	ox	H, His^-; H326, H325, H276 (*30*)
1431	Cu_A	ox	W, Trp-NH; δ(CH), ν(CC), ν(CN); W121/D, Asp-COOH; δ(COH); D178/E, Glu-COO^-; $\nu_s(COO^-)$; E218 (*28*)
1419	Cu_A	red	W, Trp-NH; δ(NH), ν(CC), δ(CH); W121/H, HisH; ν(CN), δ(NH), $\delta_s(CH_x)$; H181, H224/D, Asp-COOH; δ(COH); D178 (*28*)
1407	Cu_A	red	E, Glu-COO^-; $\nu_s(COO^-)$; E218/D, Asp-COO^-; $\nu_s(COO^-)$; D178/W, Trp-NH; ν(CC), δ(NH), δ(CH); W121 (*28*)
1389	heme *a*	ox	T; δ(COH); δ(CH); T50/E; $\gamma_w(CH_2)$; E278 (*28*)/propionate (*18*)
1354	heme a_3	red	W; ν(CC), ν (CN), δ(CH); W164, W272/Y; $\gamma_w(CH_2)$; Y280 (*28*)/ A_{1g}, ν_4 (*29*)
1332	Cu_B	ox	W; $\gamma_w(CH_2)$; W272/Y, Tyr-O^-; $\gamma_w(CH_2)$; Y280/D, Asp-COOH; δ(COH); D399/T; δ(COH), δ(CH); T344 (*28*)
1321	Cu_B	red	W; δ(CH); W272/Y; $\delta(CH_2)$ (tail group), ν(CC) δ(CH); Y280/T; δ(COH), δ(CH); T344/D, Asp-COOH; δ(COH); D399 (*28*)
1308	Cu_B	ox	D, Asp-COOH; δ(COH); D399/W; ν(CC); W272/T; δ(COH), δ(CH); T344/H, HisH; ν(C═N), ν(CN); H326, H325 (*28*)
1250	Cu_B	red	W; ν(CC), δ(CH), $\gamma(CH_2)$ (tail group); W272/T; δ(COH), δ(CH); T344 (*28*)
1151	heme *a*	red	E, Glu-COOH; ν(CO) E278/H, His H; ν(CN), δ(NH); H94, H413 (*28*)
1128	Cu_B	red	D, Asp-COOH; ν(CO) D399/W, Trp-NH; ν(CC), δ(CH); W272/T; ν(CO); T344 (*28*)
1105	Cu_B	ox	H; ν(CN), δ(CH); H326, H325, H276/Y; $\gamma(CH_2)$ (tail group); Y280 (*28*)
1032	Cu_B	ox	H_2O; H^+-oscillation; $H^+ \times (H_2O)_n$, $n = 2, 6$ (*31*)
		(b) 4000−2500 cm^{-1} Region	
3092	Cu_B	ox	OH, OH^-; ν(OH); CuB OH^- ligand/Y; ν(OH); Y280/ H; ν(NH); H326, H325/(CH) alkenes; ν(C═H); H326, H325, H276, W272, Y280
2876	Cu_B	ox	OH, OH^-; ν(OH); CuB OH^- ligand/Y; ν(OH); Y280/ H; ν(NH); H326, H325/(CH) alkanes; ν(CH); any ligand/H_3O^+; ν_{as}(OH); $H^+ \times (H_2O)_n$, $n = 5$ (*31*)

[a] Nomenclature: ν, stretching vibration; ν_s, symmetric stretching vibration; ν_{as}, asymmetric stretching vibration; δ, in-plane bending vibration; γ_w, wagging vibration; A_{1g}, ν_3, A_{1g}, ν_4, ν_{38y}, ν_{38s}, heme vibrations; CH_x, CH_2 group in 4-ethylimidazole and CH_3 group in 4-methylimidazole; *n*, number of water molecules in $H^+ \times (H_2O)_n$ cluster. [b] Alternative assignments are separated by a solidus.

redox-dependent entrance of water molecules, as described in ref *23*.

DISCUSSION

Titration of the Redox Centers in CcO. Redox titration of the peaks in the infrared has great advantage compared to the visible region because the number of bands corresponding to redox transitions of any redox center is much larger. Averaging a large number of bands, even if the majority of them overlap a little with the bands of other centers, gives a more objective picture than the two strongly overlapping bands in the visible region (Soret and α). Furthermore, the titration of the Cu_B center, invisible by UV−vis spectroscopy, shows 12 bands (see Table 2) that reflect oxidoreduction of

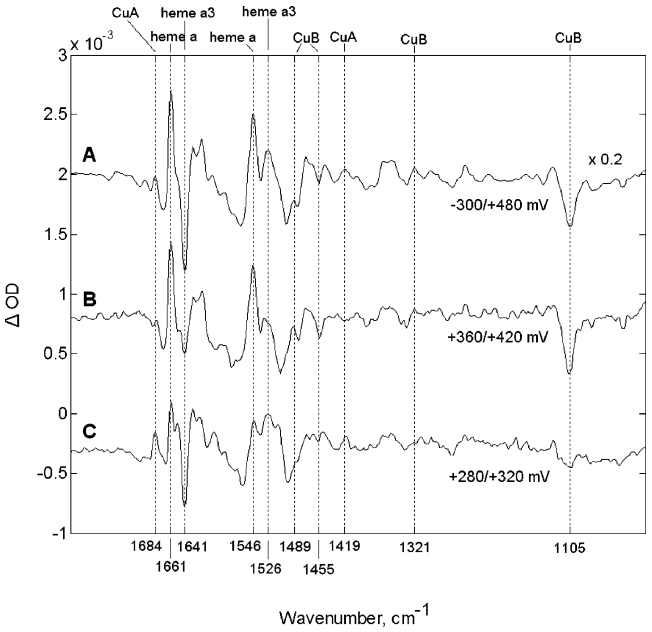

FIGURE 6: (A) Complete red-ox FTIR difference spectrum (−300 minus +480 mV) reduced five times to be comparable with (B) and (C). (B) Difference FTIR spectrum representing a potential step between +360 and +400 mV. (C) Difference FTIR spectrum representing a potential step between +280 and +320 mV. All spectra are at pH 6.5.

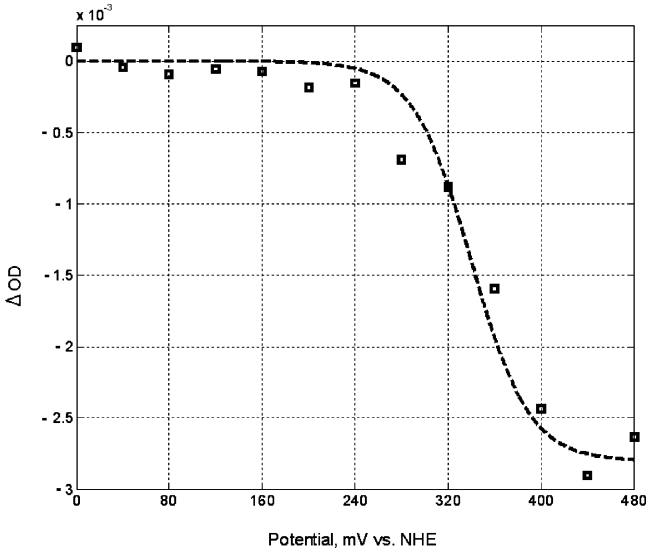

FIGURE 7: Redox titration of the continuum shift in the water region at pH 8.0. The titration curve of the shift was extracted and analyzed as described in Results.

this center, even though these bands are not as large as some of the heme bands.

Titration of the IR bands that we ascribe to be linked to heme *a* and a_3, respectively, shows clear splitting into high- and low-potential parts. Such behavior was earlier found by optical spectroscopy in the mammalian enzyme and explained in terms of redox interaction; i.e., the redox potential of one heme is lowered by reduction of the other (*19*, *20*). This interpretation is at variance with the conclusion by Hellwig et al. (*26*), who ascribed the two main optically observed redox transitions in the *Paracoccus* enzyme to hemes *a* and a_3, respectively, without redox interactions and interpreted their FTIR data accordingly. The FTIR titrations reported here do not support such a model, because a large number of infrared vibrations showed a two-potential interactive behavior, which would not be expected if the two hemes would titrate at widely separate potentials without redox interaction. In contrast to the mammalian enzyme, where the amplitudes for the high- and low-potential waves are about the same for both hemes, in *Paracoccus* the high-potential wave for one heme represents 3/5 and the other 2/5 (Figure 5A,B). This ratio would correspond to an equilibrium constant of 1.5 for electron transfer between them and a 10 mV difference in their midpoint redox potentials. We have assigned all bands with the larger amplitude of the high-potential transition to heme *a* (Figure 5A), because the titration at 605 nm, where heme *a* absorbance dominates over heme a_3, clearly shows a larger fraction of the high-potential transition. Detailed analysis of the UV−vis data on *P. denitrificans* C*c*O will be published separately (Bloch et al., to be submitted for publication).

Application of the thermodynamic model with redox interaction between hemes for the fit of the experimental data allows us to estimate not only the E_m values for the hemes at each pH but also the extent of the redox interaction in every case. The pH dependence of the E_m is −30 mV/pH for both hemes. The simple model of two redox centers with a common protonatable group, which takes a proton upon reduction of either heme (*20*), precisely describes this situation. Thus we conclude that reduction of either heme *a* or a_3 is coupled to protonation of a single common group.

The difference between the E_m values for the two hemes characterizes the equilibrium constant of electron transfer between them. From the data in Table 1 it is clear that the equilibrium constant ($K \sim 1.5$) is pH-independent in the whole investigated pH range (6.5−9.0). Such pH independence can have two possible reasons. First, the shift of the p*K* of the group that accepts the proton is the same whether heme *a* or a_3 is reduced. This would suggest that the acidic group is located at an equal distance from both hemes. The second possibility is that the p*K* value for the oxidized enzyme is at least one pH unit lower than the low border of the investigated range and at least one pH unit higher than the upper border when either heme is reduced.

Surprisingly, the redox interaction between the hemes has a pH dependence that is opposite to the one expected if the negative cooperativity were of a simple and purely electrostatic origin. Indeed, if the decrease in E_m of one of the hemes would be the result of a Coulombic interaction with the electron located at the neighbor heme, charge compensation of the latter by the binding of the proton would be less the higher the pH. Thus a simple electrostatic interaction would be expected to increase with pH, but the opposite was found. Therefore, other possible explanations for the anticooperativity should be considered. For example, the proximal histidine ligands of hemes *a* and a_3 are located on opposite sides of the same transmembrane helix, so that their relative position is fixed. Reduction of one of the hemes might create a small displacement of the imidazole ring of its proximal ligand, and this movement may be transmitted to the ligand of the other heme.

Assignment of Differential FTIR Bands in Red-Ox Spectra. The well-known redox-dependent band shift at 1737/1746 cm^{-1} has been assigned to changes in the environment of the protonated carboxyl group of E278 (*24*). Here we show that this shift correlates with oxidoreduction of heme *a*. This

is surprising at first sight because E278 is equidistant from the two heme groups. Possibly, the carboxyl group of E278 is sensitive to a redox state-dependent arrangement of water molecules in the vicinity (see ref *25*), or this group may itself be oriented in a redox-dependent fashion relative to adjacent water molecules. The largest maximum at 1661 cm^{-1} showed heme *a* oxidoreduction behavior, and the adjacent minimum at 1641 cm^{-1} reflects heme a_3 oxidoreduction. The assignment of the 1641 cm^{-1} band is in agreement with a previous assignment for bovine oxidase (*11*), but our assignment of both these bands is opposite to that in ref *26*. Previous assignments of infrared differential bands in red-ox spectra were originally based on resonance Raman data on bovine C*c*O. The band intensities of Raman spectra are relative while they are absolute in IR. Band intensities in the two methods are often reciprocal. Hence, if two bands from different redox components are at the same frequency, they may be differently emphasized in FTIR and Raman spectra, which may explain the different interpretation in this work compared to that in ref *26*.

*Deprotonation Reactions in C*c*O in the pH Range 6.5*−*9.0.* No disappearing or appearing new bands were found within the pH range 6.5−9.0. The intensities of the majority of the bands (normalized by the global peak difference 1661/1641 cm^{-1} red-ox FTIR spectra) differed within 25% at the employed pH values. However, several bands were found to be twice as small in intensity at pH 6.5 compared to pH 9.0. Redox titration of most of them reflected Cu_B reduction (the positions of these bands were 1489, 1483, 1321, and 1308 cm^{-1}); three of these bands showed Cu_A redox-dependent behavior (1603, 1468, and 1431 cm^{-1}), and one band titrated as heme a_3 (1473 cm^{-1}). These infrared bands may reflect protonation reactions of C*c*O. For example, the two bands at 1489 and 1308 cm^{-1} may be attributed to histidine ligands of Cu_B which have been proposed to take part in H^+ translocation (*27*). However, this pH-induced difference in band intensities may be caused by the normalization (which is imperfect) of titration surfaces to the global peak difference (1661/1641 cm^{-1}) and by the fact that the high-potential titration region was limited to +480 mV (for details, see Assignment of FTIR Redox Titration Curves in the 1800−1000 cm^{-1} Region). For example, bands assigned to Cu_A (1603, 1468, and 1431 cm^{-1}) are unlikely to demonstrate protonation/deprotonation behavior of surrounding ligands due to the pH-independent E_m.

In conclusion, in this study complete redox titrations of the enzyme by ATR-FTIR spectroscopy have been performed for the first time. The titrations revealed the possibility of measuring transitions of all four redox centers separately (including those "invisible" by other spectroscopic techniques, such as Cu_B). This approach allows a direct estimate of the thermodynamic constants such as the E_m values and the redox interactions, which are necessary for the construction of a thermodynamic model of C*c*O functioning. However, we stress that these values are model-dependent. In this work we present the simplest model, which only allows a redox interaction between the hemes. Inclusion of a possible interaction between Cu_B and the hemes would change these values, and further work is required to assess this possibility. However, our current approach demonstrates a new way of assigning the infrared bands of redox-active enzymes. Practically all infrared bands in the redox difference FTIR spectra of C*c*O were found to be complex, but with one major component in each. Most of these bands could be assigned to specific vibrations of the redox centers themselves and their ligands.

ACKNOWLEDGMENT

We thank Nikolay Belevich for excellent technical support, Peter R. Rich for invaluable help in setting up the ATR technique, Anne Puustinen for discussion and samples of *Paracoccus* enzyme, and Markus Kaukonen for help with data analysis.

REFERENCES

1. Babcock, G. T., and Wikström, M. (1992) Oxygen activation and the conservation of energy in cell respiration, *Nature 356*, 301−309.
2. Michel, H., Behr, J., Harrenga, A., and Kannt, A. (1998) Cytochrome *c* oxidase: structure and spectroscopy, *Annu. Rev. Biophys. Biomol. Struct. 27*, 329−356.
3. Wikström, M. (2004) Cytochrome *c* oxidase: 25 years of the elusive proton pump, *Biochim. Biophys. Acta 1655*, 241−247.
4. Brzezinski, P. (2004) Redox-driven membrane-bound proton pumps, *Trends Biochem. Sci. 29*, 380−387.
5. Iwata, S., Ostermeier, C., Ludwig, B., and Michel, H. (1995) Structure at 2.8 Å resolution of cytochrome *c* oxidase from *Paracoccus denitrificans*, *Nature 376*, 660−669.
6. Tsukihara, T., Shimokata, K., Katayama, Y., Shimada, H., Muramoto, K., Aoyama, H., Mochizuki, M., Shinzawa-Itoh, K., Yamashita, E., Yao, M., Ishimura, Y., and Yoshikawa, S. (2003) The low-spin heme of cytochrome *c* oxidase as the driving element of the proton-pumping process, *Proc. Natl. Acad. Sci. U.S.A. 100*, 15304−15309.
7. Braiman, M. S., Mogi, T., Marti, T., Stern, L. J., Khorana, H. G., and Rothschild, K. J. (1988) Vibrational spectroscopy of bacteriorhodopsin mutants: light-driven proton transport involves protonation changes of aspartic acid residues 85, 96, and 212, *Biochemistry 27*, 8516−8520.
8. Iwaki, M., Yakovlev, G., Hirst, J., Osyczka, A., Dutton, P. L., Marshall, D., and Rich, P. R. (2005) Direct observation of redox-linked histidine protonation changes in the iron-sulfur protein of the cytochrome bc_1 complex by ATR-FTIR spectroscopy, *Biochemistry 44*, 4230−4237.
9. Radresa, O., Raussens, V., Ruysschaert, J. M., and Goormaghtigh, E. (2003) Protonation of the *Neurospora crassa* plasma membrane H^+-ATPase as a function of pH monitored by ATR-FTIR, *Ann. N.Y. Acad. Sci. 986*, 347−348.
10. Scheirlinckx, F., Buchet, R., Ruysschaert, J. M., and Goormaghtigh, E. (2001) Monitoring of secondary and tertiary structure changes in the gastric H^+/K^+-ATPase by infrared spectroscopy, *Eur. J. Biochem. 268*, 3644−3653.
11. Rich, P. R., and Breton, J. (2002) Attenuated total reflection Fourier transform infrared studies of redox changes in bovine cytochrome *c* oxidase: resolution of the redox Fourier transform infrared difference spectrum of heme a_3, *Biochemistry 41*, 967−973.
12. Iwaki, M., Andrianambinintsoa, S., Rich, P., and Breton, J. (2002) Attenuated total reflection Fourier transform infrared spectroscopy of redox transitions in photosynthetic reaction centers: comparison of perfusion- and light-induced difference spectra, *Spectrochim. Acta, Part A 58*, 1523−1533.
13. Riistama, S., Laakkonen, L., Wikström, M., Verkhovsky, M. I., and Puustinen, A. (1999) The calcium binding site in cytochrome aa_3 from *Paracoccus denitrificans*, *Biochemistry 38*, 10670−10677.
14. Iwaki, M., Puustinen, A., Wikström, M., and Rich, P. R. (2003) ATR-FTIR spectroscopy of the P(M) and F intermediates of bovine and *Paracoccus denitrificans* cytochrome *c* oxidase, *Biochemistry 42*, 8809−8817.
15. Vuorilehto, K., Lütz, S., and Wandrey, C. (2004) Indirect electrochemical reduction of nicotinamide coenzymes, *Bioelectrochemistry 65*, 1−7.

16. Behr, J., Michel, H., Mantele, W., and Hellwig, P. (2000) Functional properties of the heme propionates in cytochrome *c* oxidase from *Paracoccus denitrificans*. Evidence from FTIR difference spectroscopy and site-directed mutagenesis, *Biochemistry 39*, 1356−1363.
17. Hellwig, P., Soulimane, T., Buse, G., and Mantele, W. (1999) Similarities and dissimilarities in the structure-function relation between the cytochrome oxidase from bovine heart and from *Paracoccus denitrificans* as revealed by FT-IR difference spectroscopy, *FEBS Lett. 458*, 83−86.
18. Behr, J., Hellwig, P., Mantele, W., and Michel, H. (1998) Redox dependent changes at the heme propionates in cytochrome *c* oxidase from *Paracoccus denitrificans*: direct evidence from FTIR difference spectroscopy in combination with heme propionate ^{13}C labeling, *Biochemistry 37*, 7400−7406.
19. Nicholls, P., and Petersen, L. C. (1974) Haem-haem interactions in cytochrome aa_3 during the anaerobic-aerobic transition, *Biochim. Biophys. Acta 357*, 462−467.
20. Wikström, M., Krab, K., and Saraste, M. (1981) *Cytochrome Oxidase*−*A Synthesis*, Academic Press: New York.
21. Zickermann, V., Verkhovsky, M., Morgan, J., Wikström, M., Anemuller, S., Bill, E., Steffens, G. C. M., and Ludwig, B. (1995) Perturbation of the Cu_A site in cytochrome-*c* oxidase of *Paracoccus denitrificans* by replacement of Met227 with isoleucine, *Eur. J. Biochem. 234*, 686−693.
22. Wang, H., Blair, D. F., Ellis, W. R., Jr., Gray, H. B., and Chan, S. I. (1986) Temperature dependence of the reduction potential of Cu_A in carbon monoxide inhibited cytochrome *c* oxidase, *Biochemistry 25*, 167−171.
23. Kornblatt, J. A., Hill, B. C., and Marden, M. C. (2003) The influence of temperature and osmolyte on the catalytic cycle of cytochrome *c* oxidase, *Eur. J. Biochem. 270*, 253−260.
24. Puustinen, A., Bailey, J. A., Dyer, R. B., Mecklenburg, S. L., Wikström, M., and Woodruff, W. H. (1997) Fourier transform infrared evidence for connectivity between Cu_B and glutamic acid 286 in cytochrome bo_3 from *Escherichia coli*, *Biochemistry 36*, 13195−13200.
25. Wikstrom, M., Verkhovsky, M. I., and Hummer, G. (2003) Water-gated mechanism of proton translocation by cytochrome *c* oxidase, *Biochim. Biophys. Acta 1604*, 61−65.
26. Hellwig, P., Grzybek, S., Behr, J., Ludwig, B., Michel, H., and Mantele, W. (1999) Electrochemical and ultraviolet/visible/infrared spectroscopic analysis of heme *a* and a_3 redox reactions in the cytochrome *c* oxidase from *Paracoccus denitrificans*: separation of heme *a* and a3 contributions and assignment of vibrational modes, *Biochemistry 38*, 1685−1694.
27. Popovic, D. M., and Stuchebrukhov, A. A. (2004) Proton pumping mechanism and catalytic cycle of cytochrome *c* oxidase: Coulomb pump model with kinetic gating, *FEBS Lett. 566*, 126−130.
28. Barth, A. (2000) The infrared absorption of amino acid side chains, *Prog. Biophys. Mol. Biol. 74*, 141−173.
29. Babcock, G. T., and Callahan, P. M. (1983) Origin of the cytochrome *a* absorption red shift: a pH-dependent interaction between its heme *a* formyl and protein in cytochrome oxidase, *Biochemistry 22*, 452−461.
30. Rich, P. R., and Iwaki, M. (2005) *Infrared Protein Spectroscopy as a Tool to Study Protonation Reactions Within Proteins*, pp 314−333, RSC Publishing: Cambridge, U.K.
31. Headrick, J. M., Diken, E. G., Walters, R. S., Hammer, N. I., Christie, R. A., Cui, J., Myshakin, E. M., Duncan, M. A., Johnson, M. A., and Jordan, K. D. (2005) Spectral signatures of hydrated proton vibrations in water clusters, *Science 308*, 1765−1769.

BI060257V